Diurnal and Seasonal Cycles of Cloud Occurrences, Types, and Radiative Impact over West Africa

DOMINIQUE BOUNIOL, FLEUR COUVREUX, PIERRE-HONORÉ KAMSU-TAMO, MADELEINE LEPLAY, FRANÇOISE GUICHARD, AND FLORENCE FAVOT

GAME-CNRM, CNRS-Météo-France, Toulouse, France

EWAN J. O'CONNOR

University of Reading, Reading, United Kingdom, and Finnish Meteorological Institute, Helsinki, Finland

(Manuscript received 2 March 2011, in final form 26 July 2011)

ABSTRACT

This study focuses on the occurrence and type of clouds observed in West Africa, a subject that has been neither much documented nor quantified. It takes advantage of data collected above Niamey, Niger, in 2006 with the Atmospheric Radiation Measurement (ARM) Mobile Facility. A survey of cloud characteristics inferred from ground measurements is presented with a focus on their seasonal evolution and diurnal cycle. Four types of clouds are distinguished: high-level clouds, deep convective clouds, shallow convective clouds, and midlevel clouds. A frequent occurrence of the latter clouds located at the top of the Saharan air layer is highlighted. High-level clouds are ubiquitous throughout the period whereas shallow convective clouds are mainly noticeable during the core of the monsoon. The diurnal cycle of each cloud category and its seasonal evolution are investigated. *CloudSat* and *Cloud–Aerosol Lidar and Infrared Pathfinder Satellite Observations* (*CALIPSO*) data are used to demonstrate that these four cloud types (in addition to stratocumulus clouds over the ocean) are not a particularity of the Niamey region and that midlevel clouds are present over the Sahara during most of the monsoon season. Moreover, using complementary datasets, the radiative impact of each type of clouds at the surface level has been quantified in the short- and longwave domains. Midlevel clouds and anvil clouds have the largest impact, respectively, in longwave (about 15 W m^{-2}) and shortwave (about 150 W m^{-2}) radiation. Furthermore, midlevel clouds exert a strong radiative forcing during the spring at a time when the other cloud types are less numerous.

1. Introduction

Several authors (Cess et al. 1996; Dufresne and Bony 2008) have invoked clouds as a major source of uncertainty for future climate projections, in particular through a diversity of feedbacks between clouds and radiative processes. Furthermore, clouds also strongly affect weather forecasts and play an important role in the water cycle. In the tropics, a majority of cloud studies have focused on oceanic regions, and much less is known and understood about clouds occurring over continental regions. This is particularly true in areas where data are sparse, like West Africa.

During the monsoon season (June–September) in West Africa the rain originates mainly from mesoscale convective systems (Mathon et al. 2002). These convective systems are often associated with extended anvils (Leary and Houze 1979; Gamache and Houze 1983; Houze 2004) located in the upper troposphere. However, very little is known about other cloud systems occurring in this region or about cloud systems occurring before the monsoon onset. Major advances in the documentation of the cloud occurrence, diurnal cycles, or intraseasonal variations were achieved from the Global Atmospheric Research Program (GARP) Atlantic Tropical Experiment (GATE) and through geostationary satellite measurements (Duvel 1989). The climate of such a continental region is however expected to be sensitive to cloud feedbacks on radiative processes that are themselves affecting the surface processes and energy balance (e.g., Betts and Viterbo 2005; Betts 2007; Garratt 1993). Clouds

Corresponding author address: Dominique Bouniol, GAME-CNRM, 42 Ave. Gaspard Coriolis, 31057 Toulouse CEDEX, France.
E-mail: dominique.bouniol@meteo.fr

DOI: 10.1175/JAMC-D-11-051.1

and cloud feedbacks are thus a key component of the monsoon system that need to be better documented and understood.

A major advance over poorly documented regions was achieved in 2006 with the launch of the *CloudSat* (Stephens et al. 2002) and *Cloud–Aerosol Lidar and Infrared Pathfinder Satellite Observations* (*CALIPSO*; Winker et al. 2007) satellites that provide a cloud radar and a lidar within the A-Train constellation. This downward sampling provides bidimensional ''slices'' within cloud systems. The orbits of the constellation are sun synchronous, passing over the equator at about 0130 (night) and 1330 (day) mean local time (twice per day). The A-Train's orbit repeats approximately the same ground track every 16 days.

Figure 1 shows this 16-day ground track over a 10°W–10°E transect domain located over West Africa. In the north–south direction, this domain is sampled only twice per day (one during daytime and one during nighttime) and, because of the sun-synchronous orbit, at fixed hours. Documenting the seasonal and diurnal cloud cover evolution using the *CloudSat–CALIPSO* dataset may then be biased by this temporal subsampling.

As detailed in the following, the African monsoon is characterized by a well-defined meridional structure, in particular in surface albedo, vegetation, and atmospheric circulation, with relatively weaker longitudinal variations. This feature provides a valuable constrain for modeling and model-evaluation purposes (Zheng and Eltahir 1998; Hourdin et al. 2009). Here, we focus on the cloud cover latitudinal variations by assuming that any track in the domain shown in Fig. 1 is representative of a north–south vertical slice at 0° longitude. A daily documentation of the latitudinal cloud cover variations results from this assumption. It is further compatible with the African Monsoon Multidisciplinary Analysis (AMMA) cross-section (AMMA-CROSS) framework developed in Hourdin et al. (2009) and can be related to dynamical features described in this paper.

In coincidence with the launch of the *CloudSat* and *CALIPSO* satellites, the Atmospheric Radiation Measurement (ARM) Mobile Facility (AMF) was deployed for one year (2006) at the Niamey, Niger, airport (Miller and Slingo 2007), as part of the AMMA field experiment (Redelsperger et al. 2006; Lebel et al. 2010). The AMF is a portable facility equipped with cloud-dedicated instrumentation (vertically pointing 94-GHz radar and lidar) that provides continuous, high temporal cloud profile documentation, a radiosounding facility, and surface budget measurements. Niamey is located at 13.5°N and 2.3°E (black square in Fig. 1), which corresponds to the transition region between the Sahel and the Sahara Desert, one of the driest regions in the world. These data provide a high-frequency temporal sampling at this location that may be compared with satellite data in order to identify any possible bias related to the A-Train's much coarser sampling. Conversely, the ground-based

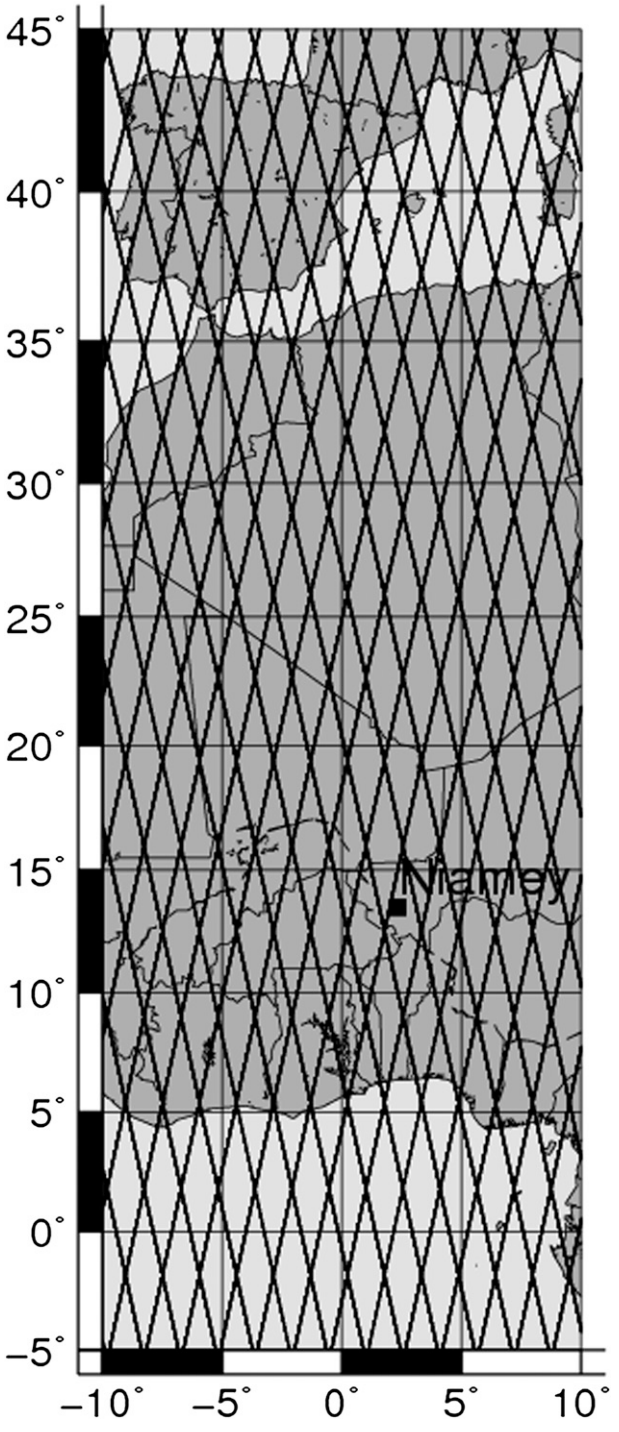

FIG. 1. Sixteen days of A-Train ground track over the AMMA-CROSS domain as defined in Hourdin et al. (2009). The black square indicates the location of Niamey (13.5°N, 2.3°W).

measurements and resulting climatology correspond to a particular location and the satellite data may be used to generalize the results obtained at this particular location to the continental scale.

Only a few recent studies have made use of the West Africa AMF dataset for climatological purposes so far. Kollias et al. (2009) analyze the relationships between clouds, precipitation, and the thermodynamical environment from daily to longer time scales without explicit consideration of cloud types. Protat et al. (2010) focused on the statistical properties of ice clouds and how they differ with those encountered over Darwin, Australia, in another monsoon region. In contrast, the purpose of this paper is first to document the cloud characteristics, the diurnal cycles, and patterns of seasonal evolution of all cloud types encountered in the Niamey region during spring and summer. This includes covering the premonsoon and monsoon periods, both of which are climatologically important and known to display distinct surface and dynamic large-scale features (Sultan and Janicot 2003).

These investigations are motivated by and useful for the following purposes. First, this research can serve as a reference to be compared with space-borne measurements or used in order to evaluate cloud classifications from geostationary satellites. Such a characterization is also useful in order to infer the ability of models, either numerical weather prediction or general circulation model, in reproducing the observed cloud seasonal and diurnal cycles. A step forward is achieved with an evaluation of the radiative impact of each cloud category on the surface radiative fluxes. This can also further be used to assess the radiative impact of each type of clouds in models.

This paper is organized as follows. Section 2 presents the data and the processing applied in order to compute the cloud frequency of occurrence at a half-hour scale. This section also presents how the data are sorted according to defined categories. The intraseasonal evolution and the diurnal cycle are then investigated in section 3. In section 4 the impact of each cloud category on the surface fluxes is quantified. Concluding remarks and perspectives are given in the last section.

2. Cloud frequency of occurrence

A detailed description of the AMF instrumentation may be found in Miller and Slingo (2007). The basic strategy of the ARM stations [Stokes and Schwartz (1994); disseminated around the globe] is to continuously collect vertical profiles of cloud properties using cloud radar (35 or 94 GHz) and lidar and to measure fluxes and meteorological variables at the surface simultaneously. These measurements were developed in the early 1990s and have since allowed us to build cloud climatologies (Protat et al. 2010; Comstock et al. 2002; Mather and McFarlane 2009) as well as to evaluate the ability of models to produce the right statistics for cloud variables (see, e.g., Hogan et al. 2001; Bouniol et al. 2010). Indeed, macrophysical (cloud frequency of occurrence, cloud-base and -top height), microphysical (ice and liquid water content), radiative (effective radius) properties, or even heating profiles (Mather and McFarlane 2009) may be derived from these measurements. This paper is mainly devoted to the documentation of cloud frequency of occurrence and cloud radiative impact on ground radiative fluxes within West Africa.

A key point lies in the definition of the cloud frequency of occurrence, even if the general definition ''number of cloudy observations to the total number of observations at each level'' is used. To do so, the data have been categorized following the process described in Illingworth et al. (2007) and fully detailed in Hogan and O'Connor (2010). This algorithm provides cloud profiles every 43 s with 60-m vertical resolution. Special care has been taken not to consider rain and drizzle as clouds (each gate of the radar–lidar profile being categorized). Therefore, only the presence of liquid droplets, ice droplets, supercooled droplets, or melting ice makes the ''pixel'' cloudy. Figure 2a shows the cloud frequency of occurrence derived from the AMF data at the Niamey site from 1 June to 30 September 2006.

Depending on the objectives, the cloud frequency of occurrence may be computed from ground-based instrumentation over different time spans. For instance, if one considers the data at full resolution (temporal and vertically; red line in Fig. 2a) a mean frequency of occurrence of approximately 8% is obtained (thin black line in Fig. 2a). This is very similar to the results obtained by Protat et al. (2010). On the other hand, for comparison with models (Hogan et al. 2001; Bouniol et al. 2010), it is necessary to compute the cloud frequency of occurrence from the observations at the model grid scale. The horizontal wind speed can be used to determine at each grid point an averaging time (see, e.g., Hogan et al. 2001) corresponding to the model horizontal resolution. The observed cloud frequency of occurrence profile is then representative of a model grid. The chosen model grid may lead to substantial differences in the profiles of the frequency of occurrence, as illustrated in Fig. 2a, where observed cloud occurrences computed using the European Centre for Medium-Range Weather Forecasts (ECMWF) grid (0.5° latitude–longitude squared and 91 vertical levels; dashed black line) or the Met Office global model grid (60-km^2 horizontal resolution and 50 vertical levels; dotted black line) are also shown. Both models

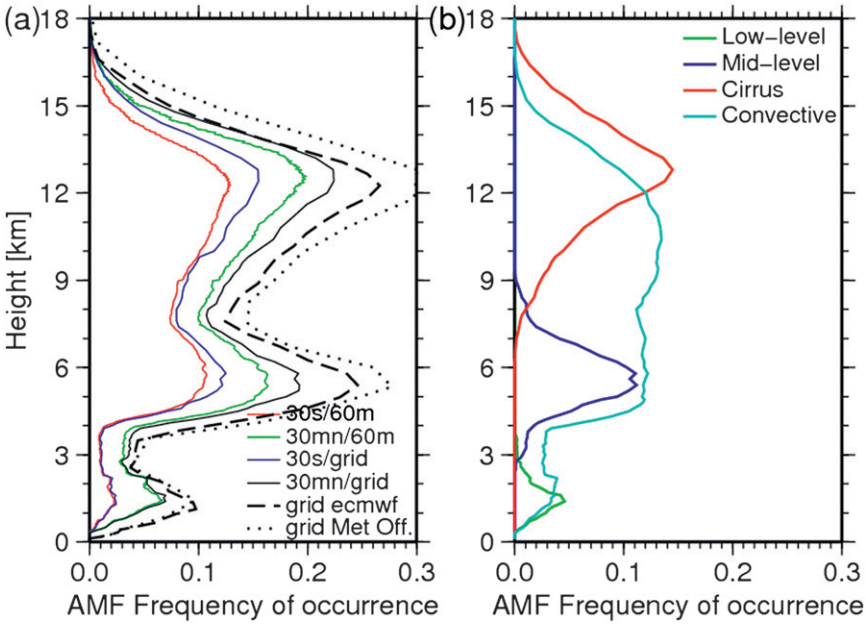

FIG. 2. (a) Cloud frequency of occurrence for the 2006 monsoon season (1 Jun–30 Sep) computed from the AMF radar–lidar at Niamey using different temporal and vertical grid resolutions (defined in text, one color for each temporal and vertical grid combination), using the ECMWF model grid (dashed black line) and the Met Office global model grid (dotted black line). (b) AMF cloud frequency of occurrence (30 min/grid) for each cloud category (see text for definitions).

also have a variable vertical resolution that has been taken into account for computing the profiles. The main conclusion arising from this comparison is that the cloud frequency of occurrence is scale dependent and no "universal" profile can be derived. Important, though, is that the broad shape and peaking levels remain identical. Xi et al. (2010) provide similar results. Namely, they stated that when comparing clouds from weather or climate models to cloud frequency of occurrence derived from data, the temporal averaging time should be matched to the size of the model resolution.

The green line is obtained by binning the data on a 30-min time base and keeping the full vertical resolution. An increase in the peak value appears relative to the red line (full resolution) because a grid box is considered cloudy as soon as some clouds have been included within it, independent of the value of the cloud fraction. This finding is in agreement with the results of Xi et al. (2010) over the southern Great Plains (see their Fig. 3). To reflect what can be found in the models, a vertical variable-resolution grid has been defined (100-m resolution below 5 km, 200 m between 5 and 10 km, and 400 m above), and the corresponding occurrence profiles with the high vertical resolution or the defined grid are shown in Fig. 2a as green and black lines, respectively. Averaging on the vertical also leads to an increase, more significant in the upper levels where the resolution is coarser, of the peak values. To truly identify the impact of changing the vertical resolution, one may also compare the red and blue profiles where the full time resolution is used, but the vertical grid is used in the blue profile computation. In the following the cloud profiles are computed with 30-min averages and on this variable vertical grid (black line).

The cloud frequency of occurrence displays three peaks: two with the same magnitude in the middle levels (7 km) and in the high level (13 km) and one of smaller magnitude in the low levels (1.5 km). A contribution between 4 and 16 km from a deep convective system is also observed. On the basis of previous studies, the three peaks identified in Fig. 2a may be associated with three different cloud categories in addition to clouds directly associated with deep convection. Kollias et al. (2009) found a bimodal structure (peaking at 11.5 and 5.5 km) for the average profile of the cloud and precipitation fraction. When exploring the seasonal evolution, we found trimodality from July to September and bimodality from April to June (see section 3).

These cloud categories were reported in previous studies. Hayward and Oguntoyinbo (1987) or Slingo (1980) proposed a general characterization of the cloud cover into West Africa that included four categories. Houze and Betts (1981) summarized the observations of

Simpson (1976), Borovikov et al. (1978), Peskow (1980), and Lebedeva and Zavelskaya (1980), who found from whole-sky camera photography in GATE a frequent presence of several cloud layers, including cumulus clouds with bases near 500 m and layer clouds with midtropospheric bases near 4 km. Holle et al. (1979) determined that the frequency of low clouds (including deep cumulus and cumulonimbus as well as stratus and stratocumulus) was maximal just south of 7°–8°N (thus about 500 km south of Niamey). Following these earlier works, we define the following categories.

- The *low-level cloud* category includes clouds with a top lower than 3 km and a base not higher than 500 m above the lifting condensation level computed from the meteorological surface measurements.
- The *midlevel cloud* category has a base between 3 and 7 km. Duvel (1989), using geostationary satellite data, noted the significant amount of this type of cloud but mentioned that the nature and the origin of these clouds are unclear.
- The *cirrus* category for clouds has a base above 8 km. Several authors [see Fueglistaler et al. (2009) for a review] mention the existence of cirrus in the tropopause transition layer [which may be optically quite thin and even subvisible; Sassen and Cho (1992); Jensen et al. (1996)]. Several explanations were invoked for their origin: either convective (Hartmann et al. 2002; Dessler and Yang 2003; Jensen et al. 1996), associated with vertically propagating Kelvin and gravity waves (Boehm and Verlinde 2000), or synoptic-scale ascent along isentropic surfaces (Pfister et al. 2001; Jensen et al. 1996).
- The last category corresponds to deep *clouds associated with convective systems*. They are first determined by using the melting layer in the radar measurement. If a cloud depth (larger than 5 km) above this melting layer is found, the profile is classified as convective and this property is propagated temporally before and after in order to include anvil clouds. The classification of nonprecipitating anvils within convective clouds may not be obvious from a vertically pointing perspective since the edge of a convective system may be classified as cirrus. In such situations, the freezing level is never identified. To avoid this issue, we use the results of a tracking algorithm (Arnaud et al. 1992; Mathon and Laurent 2001; Fiolleau et al. 2009). When a cloud is classified as cirrus, it is sought whether the corresponding location in the satellite image is associated with a tracked cell. If this is the case, the sampled cloud is reclassified in the convective category and this property is propagated temporally before and after the sampled profile.

The respective contributions of each cloud category to the mean profile (black boldface line in Fig. 2a) are shown in Fig. 2b, where the larger frequency of occurrence is attributable to cirrus clouds. At this point, the instrumental limitations must be mentioned. As the AMF instruments are sampling clouds from base to top, the vertical extension of the convective profile may be underestimated. Indeed, rain processes and water clouds strongly attenuate the radar signal and may extinguish completely the lidar signal before it reaches the cloud top (Spinhirne 1993). If one of the instruments does not present enough sensitivity to detect thin clouds, then the profile of the frequency of occurrence will be underestimated as well. To quantify this bias, the use of satellite data that sample from top to bottom (and in particular the *CALIPSO* results) is valuable. A comparison of the cloud frequency of occurrence profiles derived from AMF measurements with the one derived from A-Train data is proposed in Fig. 3.

The cloud frequencies of occurrence are shown for August (Fig. 3a) and June–September (Fig. 3b). Two years are displayed for the satellite data because, even if 2006 is of major interest because it temporarily coincided with AMF measurements, this year corresponds to the beginning of operation of the *CloudSat* radar and *CALIPSO* lidar. Therefore, some gaps exist in the 2006 dataset. Conversely, the 2008 dataset is by far more continuous. The presented A-Train profiles correspond to extraction at the latitude of Niamey (they have been computed using the strategy described in the introduction: assuming that any track within the Fig. 1 domain is representative of 0° longitude, binning the latitude in 0.1°N intervals and the altitude in 0.5-km intervals). Precipitation has been removed from the data, using the precipitation flag of the 2B-CLDCLASS *CloudSat* product. When the flag indicates precipitation, data are flagged as precipitation from the bottom up to the melting level (diagnose from the ECMWF-AUX CloudSat product) and data from contiguous profiles are also classified as precipitation as long as cloud is found above and below the melting level. As may be seen in the bottom panel in Fig. 3, about 50 profiles for 1 month (and 170 profiles for 4 months) have been used to compute the satellite occurrence profile, composed equally of daytime and nighttime profiles.

First, both the AMF and 2006 A-Train products (comparison of solid black and green lines) indicate a similar vertical structure with three different peaks. The differences in intensity between the AMF data (black line) and the satellite data (green line) occurrence profiles are linked to differences in the sampling between ground-based (temporally integrated) and satellite (spatially integrated) data. Different sensitivity tests have been

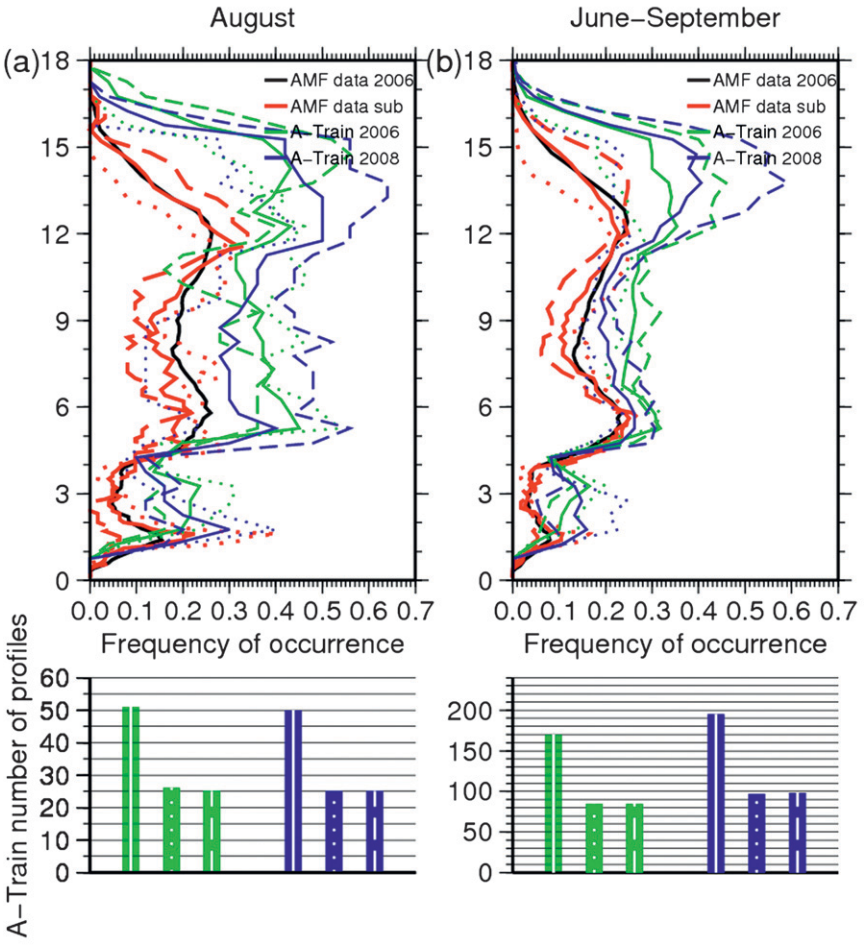

FIG. 3. Cloud frequency of occurrence (solid line) computed from the A-Train *CloudSat–CALIPSO* data for 2006 (green) and 2008 (blue) and from the AMF data (black) collected during 2006 for (a) August and (b) June–September. The AMF profile has been subsampled at the time of the A-Train passes (0130 and 1330 local time) at the Niamey latitude (red). Dashed (dotted) lines are the profiles for nighttime (daytime) datasets. The bottom panel shows the amount of satellite data included for computation of the satellite profiles for 2006 (green) and 2008 (blue) with solid, dotted, and dashed symbols for total, daytime, and nighttime datasets, respectively.

performed (not shown) in order to evaluate the impact of the domain width or bin size (horizontal and vertical). The main result from these tests is that the occurrence profiles do not change significantly when reducing the domain width. The main impact is to reduce the amount of data used in the statistics computation, which leads to noisier profiles. A larger impact is found for the size of the horizontal bin, but the vertical structure of the profile does not change. The comparison between the A-Train profiles for the 2006 (green line) and 2008 (blue line) datasets suggests that the interannual variability is relatively small.

The respective amplitudes of the peak value of the A-Train profile are useful for inferring a potential impact from the lack of sensitivity of the ground-based radar and lidar. First, the peak value for high-level clouds is higher (about 14 km) in the satellite data compared to the ground-based data (about 13 km). For both the ground-based and satellite datasets, low- and midlevel peaks present the same relative amplitudes (in Fig. 3b): about 0.1 (a slightly larger value is found for 2008) for the low-level peak and about 0.2–0.3 for the midlevel peak. In contrast the high-level peak has the same magnitude as the midlevel peak for the ground-based profile but is 50% larger for the *CloudSat–CALIPSO* profile. This result indicates that a given amount of high-level clouds is underestimated in the ground-based dataset either due to attenuation–extinction by the underlying cloud layers or

to a lack of instrumental sensitivity. The amount of high-level clouds missed due to a potential lack of sensitivity of the AMF instrumentation may be further estimated via a classification of the A-Train data according to the four previous categories. Indeed, by comparing the relative amplitude of the ''cirrus only (in the sampled column)'' occurrence profiles versus the ''cirrus and other clouds'' occurrence profiles obtained with A-Train data, one should be able to precisely identify the amount of the cirrus only situation missed by the AMF data. Such a capability using the A-Train data remains to be developed, and this constitutes a valuable perspective of the present work. From a general point of view, the comparison shown in Fig. 3 demonstrates that the methodology proposed for using the *CloudSat–CALIPSO* data is suitable for documenting the cloud cover evolution at the scale of West Africa. The comparison of the ground-based profile with the satellite profile shown in Fig. 3 allows us to evaluate possible compensating effects in the satellite mean profiles due to the temporal subsampling of the cloud system over this region. To do so, the AMF profile has been subsampled at the same times (approximately 0130 and 1330 local time) and the resulting mean profile appears as a solid red curve in Fig. 3. This presents a rather similar pattern of behavior, which suggests that even if some compensating effects occur, the main features are captured.

The AMF and A-Train datasets can also be separated between day- and nighttime profiles (dashed–dotted lines in Fig. 3) in order to infer possible diurnal fluctuations in the cloud cover. These comparisons show that important differences exist for low-level and high-level clouds with more low-level clouds during daytime and more high-level clouds during nighttime. The next section investigates further the diurnal cycle and its seasonal evolution by making use of high-frequency ground-based measurements.

3. Seasonal evolution and diurnal cycle

The West African monsoon has a strong seasonal cycle in both its surface and atmospheric large-scale properties [see, e.g., Le Barbé et al. (2002) for rainfall]. The purpose of this section is to investigate the evolution of cloud frequency of occurrence associated with the monsoon seasonal cycle. Major intense rainfalls appear near the Gulf of Guinea starting in April (with a quasi-stationary ITCZ located at 5°N), move up to 10°N during summer (with a fully developed monsoon in August), and then retreat back to the south after mid-September. This signals the seasonal march of the ITCZ (Sultan and Janicot 2000; Le Barbé et al. 2002; Redelsperger et al. 2002) between 10°W and 5°E where a meridional land–sea contrast exists. The northward migration is characterized by an abrupt shift in the major rain zone referred to as monsoon onset. Sultan and Janicot (2000) propose as a mean date for this shift over the period 1968–90: 24 June with a standard deviation of 8.0 days. In 2006 (the year of interest for this paper), the monsoon activity was less developed in June but had a similar extension when compared with the climatology in July. The monsoon onset was determined to be around 10 July 2006 (Janicot et al. 2008).

a. Seasonal evolution of the cloud frequency of occurrence

Figure 4 presents the monthly evolution of each cloud category derived from the AMF data at the Niamey site. The dotted black line corresponds to the frequency of cloud occurrence of all clouds without distinction. As expected, August (monsoon peak) is the cloudiest month, with about 0.2 of cloud frequency of occurrence. The frequency of occurrence of convective cloud (light blue) is well correlated with the monsoon seasonal cycle with a progressive increase of frequency beginning in June, peaking in August, and decreasing in September. The relatively high frequency of occurrence in May (0.1) is in fact associated with three days of convective activity (between the 19th and 21st of the month) in the Niamey area but no other convective events occurred before the beginning of June. Also well correlated with the monsoon cycle is the frequency of occurrence of low-level clouds (green), which begins in May but appears more distinctively in July, grows in August, and decreases in September. In contrast, the peak in frequency of occurrence of midlevel clouds (blue line in Fig. 4) is observable for each month without evident links with the monsoon cycle. As stressed by Duvel (1989), the processes that generate such midlevel clouds are questionable. Johnson et al. (1999) investigated the thermodynamical environment in which such midlevel clouds occur (they are termed congestus in their paper). They showed that they are often associated with a stable layer whose strength appears sufficient to delay or limit cloud growth and to promote detrainment near those levels. However here, such clouds are already present in the preonset period (April–May) when very few convective systems occurred. This contrasts with the results of Johnson et al. (1999), who relate these clouds to deep convective activity and melting. Finally, cirrus clouds (red line) are present in all months but with a distinct maximum in May. To compare the macrophysical properties of cirrus clouds (red line in Fig. 4) with nonprecipitating high clouds generated by convective activity (anvils), the convective category has been divided into two subcategories: anvils (dashed light-blue line) and precipitating clouds (dotted light-blue

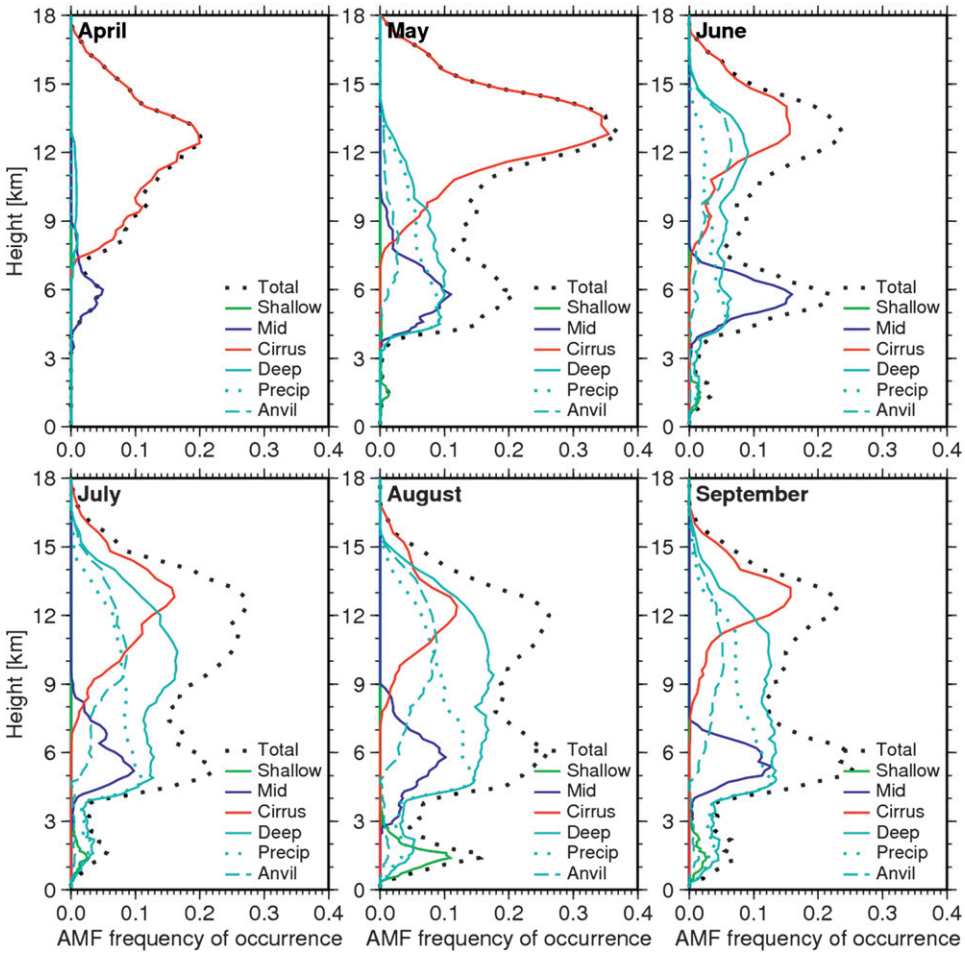

FIG. 4. Seasonal evolution of the cloud frequency of occurrence (April–September 2006) for each cloud category (one color per category) derived from the AMF data.

line). The frequencies of occurrence of cirrus and anvils present different shapes and amplitudes: the cirrus profiles always peak higher (about 13-km altitude) than the anvils profiles (about 10 km) and they are always more frequent. In addition, it has been demonstrated, using satellite data, that this frequency is certainly underestimated.

As proposed in the previous section, one may try to generalize the results obtained at the Niamey site to the West Africa scale by using the satellite data. Figure 5 shows monthly latitude–altitude cross sections of cloud frequency of occurrence between 5°S and 45°N derived from A-Train data. The Niamey latitude is shown by the vertical dotted line, and the two dashed lines roughly correspond to the Guinea coast and the limit of the Mediterranean Sea. Only the 2008 seasonal cycle is shown here in order to be able to document the premonsoon period (data in 2006 were only available after 15 June).

The monsoon jump is observable between June and July with a northward shift of the cloud cover following the motion of the ITCZ. The cloud categories identified in section 2 in the AMF data are observable along these cross sections. High-level clouds present the strongest occurrence during the premonsoon period, and extend from the Atlantic Ocean up to the Sahel where the Niamey site is located. During this period, 5°N corresponds to the location where most convective events occur. In June the ITCZ is still located in the area of the Guinea Gulf but with a strong decrease in the occurrence of these high-level clouds, in particular over the ocean, which suggests that these clouds do not only have a purely convective origin. This decrease in high-level cloud over the ocean (and south of the convective activity zone) continues as the convective activity moves northward. Midlevel clouds consistently extend across West Africa, and notably over the Sahara between May and September. Finally, low-level clouds appear to be

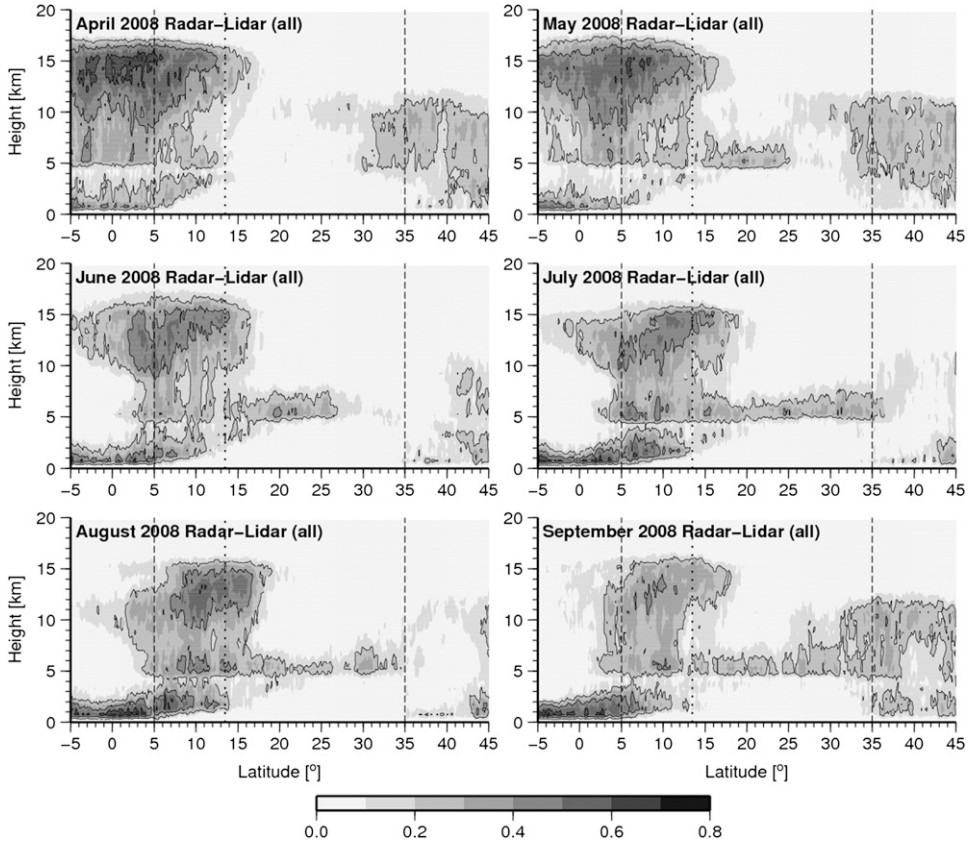

FIG. 5. Monthly latitude–altitude cross sections of cloud frequency of occurrence (shaded) computed from the *CloudSat* radar and *CALIPSO* lidar data between 10°E and 10°W for the 2008 monsoon season. Vertical dashed lines correspond to the mean positions of the Guinea Gulf (5°N) and the Mediterranean Sea (35°N). Dotted line shows the latitude of Niamey (13.5°N).

clearly tied to the monsoon cycle with a frequency that becomes more substantial over the continent after the monsoon jump. One may also note the strong occurrence of low-level clouds over the ocean (stratocumulus) before and during the monsoon.

b. Seasonal evolution of the cloud frequency of occurrence diurnal cycle

In this section the diurnal cycle of each cloud category is investigated as a function of the monsoon evolution using a monthly time step and is presented in Fig. 6 (for convection subdivided in precipitating in filled contours and anvil in solid line contours) and Fig. 7 (for low-level cloud in green, midlevel cloud in blue, and cirrus in red). These figures show the cloud frequency of occurrence from AMF data of a given cloud category as a function of altitude and hour in daytime. It appears that all cloud categories display a diurnal cycle evolving from month to month.

Precipitating convection (Fig. 6) occurs almost exclusively in the evening, after 1800 UTC in June at Niamey, and anvils (open contours) are strongly tied to this maximum of occurrence of precipitating clouds (i.e., they do not persist for long periods of time after the precipitating convection occurred). This observation is in agreement with a predominance of the small-sized minimally propagating convective events, mostly driven by the diurnal cycle of surface and boundary layer processes; since over land daytime heating exerts the primary control on the diurnal cycle of precipitating convection (Johnson et al. 2010). Further, during the monsoon season (July–August) two peaks appear in the diurnal cycle: one centered in the afternoon and the other in the morning. This picture is consistent with the results of Rickenbach et al. (2009). They show that the afternoon peak may be associated, as in June, with locally generated convection. The earlier occurrence of this afternoon peak as the season evolves is possibly due to a moister boundary layer enabling an earlier triggering of convective processes. On the other hand, the morning peak is associated with propagating systems initiated during the afternoon over the relief east of the Niamey

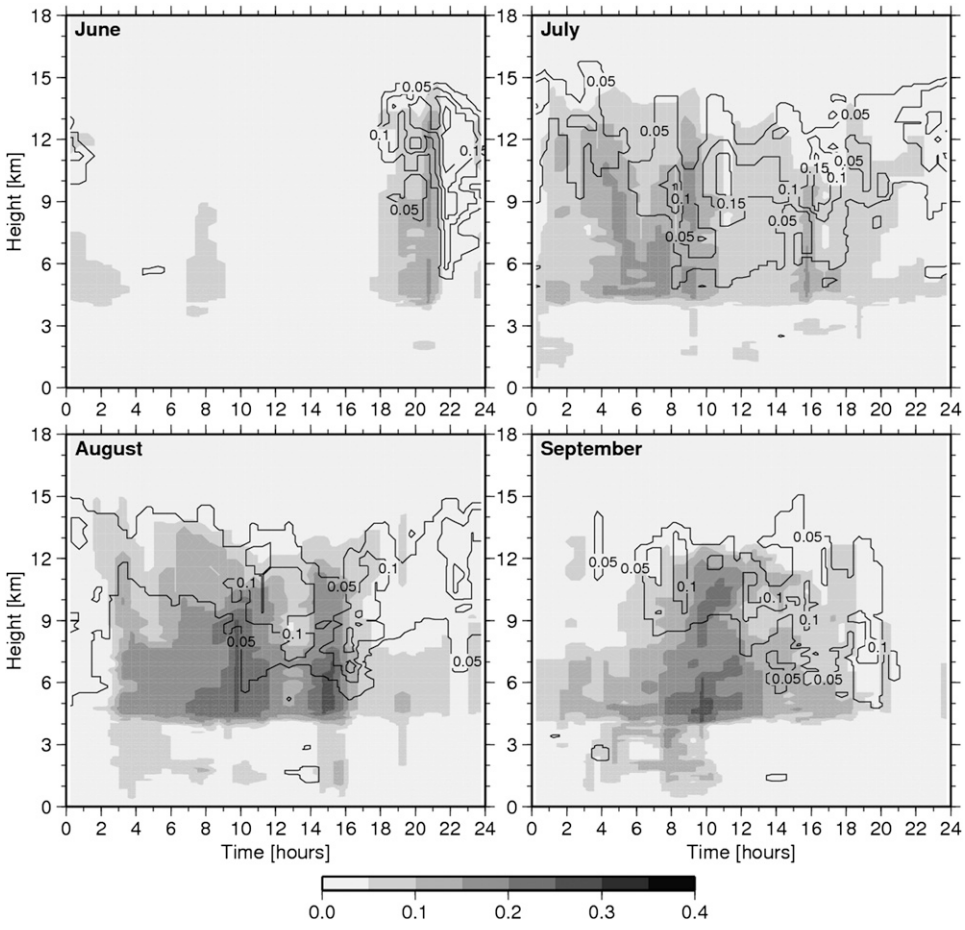

FIG. 6. Monthly diurnal cloud frequency of occurrence derived from AMF data for convective cloud types subdivided in two subcategories: clouds that lead to precipitation (open contours; grayscale) and clouds that do not lead to precipitation (anvils; solid lines, spaced every 0.05). May has not been included because the cloud category for this month is only available for 3 days.

region (Mathon et al. 2002; Diongue et al. 2002). Using back trajectories, Rickenbach et al. (2009) determine that they are generated the day before (between 1200 and 1800 UTC) in the Aïr Mountains and the Jos Plateau. Extended anvils follow these precipitating cloud systems. In September it is mainly the morning peaks that remain (associated with following extended anvils), suggesting fewer occurrences of local generated convective systems. This pattern of behavior is clearly shown in Fig. 4b of Rickenbach et al. (2009).

The growth of the boundary layer linked to the daytime increase of sensible heat flux is well observable on the diurnal cycle of low-level clouds (green contours in Fig. 7) and, as already mentioned in Fig. 4, is correlated with the mature monsoon. The maximum of occurrence is found in August with a diurnal cycle clearly identifiable since July. These clouds appear earlier in August in agreement with a moister boundary layer at the Niamey location, leading to a lower lifting condensation level (corresponding approximately to the cloud base) and deeper clouds. Once the monsoon begins to retreat (southward motion of the monsoon flux in September), a diurnal cycle somewhat similar to that observed in July returns.

Midlevel clouds (blue contours in Fig. 7) present a maximum of occurrence in the early morning and then a daytime decrease (except in August) until about 1900 UTC. These clouds generally occurred around the top of the Saharan air layer, which also corresponds to a maximum in the relative humidity profiles. A visual inspection of the AMF data suggests that these clouds may have been generated through different processes (not shown). In some occasions, they appear deeper (altocumulus type) and may lead to evaporating precipitation, in contrast to the congestus of Johnson et al. (1999), which may lead to substantial precipitation. On other occasions, they appear rather thin and horizontally extended, often located at the top of the Saharan air layer. According

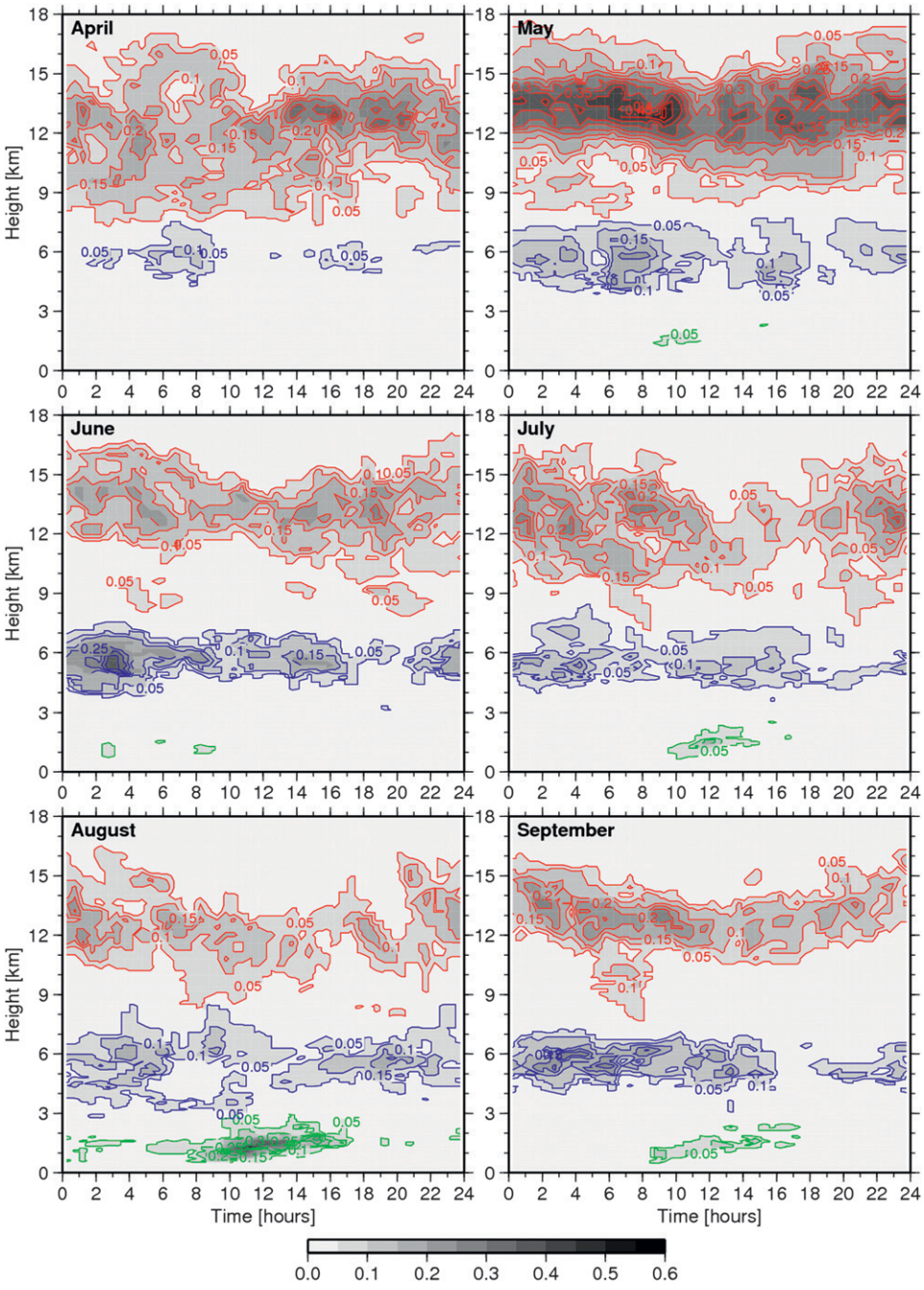

FIG. 7. As in Fig. 6, but for nonconvective cloud categories: cirrus cloud (red contours), midlevel clouds (blue contours), and boundary layer clouds (green contours), and one panel per month. A contour is shown for every 0.05.

to their altitudes, they are expected to be mixed-phase clouds.

Finally, cirrus clouds (red contours in Fig. 7) occur all day long at Niamey. A noticeable feature appears, on the diurnal cycle of this cloud category, with a decrease in cloud-top altitude around the middle of the day, while the distribution of the frequency of occurrence at the cloud base remains unchanged. The time location of this decrease in cloud-top altitude evolves during the season (from about 1200 UTC in April to 1500 UTC in August). Between 9 and 12 km, the AMF lidar is generally necessary to detect these relatively optically thin clouds.

However, during the day the lidar experiences a drop in its sensitivity due to solar background noise (Spinhirne 1993) causing the undetectability of thin cirrus during daylight hours. It is then questionable to determine if the observation of this trough is in fact an observation of the lidar sensitivity diurnal cycle. This diurnal cycle must then be determined in independent datasets that are insensitive to the diurnal cycle. Unfortunately, the cloud radar sensitivity was not sufficient to characterize the diurnal evolution of these thin cirrus (not shown).

Nevertheless, during the AMMA experiment the radiosounding network has been substantially reinforced, which provides an additional way to investigate this diurnal feature. In particular, at the Niamey location four soundings per days were launched during the synoptic hours. The AMMA radiosonde dataset has been corrected to minimize any potential humidity bias. A conditional sampling has been applied to this dataset in order to sort it in three subsets: measurements in clear sky, measurements in a single cloud category (cirrus in the present case), and measurements in other cloud categories or multi-cloud-categories situations. The whole troposphere is sampled within about 1.5 h by sondes, which simultaneously drift horizontally with the wind. It is then difficult to consider that the atmospheric column sampled at the Niamey location by the ground-based instrumentation is the same as that sampled by the sondes. However, the cloud category of interest (cirrus) generally presents a large horizontal extent and slowly evolves (this point has been checked in geostationary imagery). The hypothesis that the sonde thermodynamical profiles, once sorted, are characteristic of cirrus or clear-sky situations is then assumed.

Figure 8 shows the monthly mean diurnal cycle of cloud frequency of occurrence from AMF data for the cirrus category with the contoured relative humidity anomaly from interpolated radiosondes (relative humidity with respect to ice in cirrus situations minus relative humidity with respect to ice in clear-sky situations) superimposed. A positive anomaly means that the cloudy situations present higher relative humidity with respect to the clear-sky situations. As expected, the larger values of the anomalies are generally found in the cloud layer. Close to cloud top, the relative humidity anomaly presents a diurnal cycle similar to cirrus, with a decrease in the anomaly around the middle of the day. The minimum cannot be located with accuracy since these contours result from an interpolation of values obtained at the synoptic times (0000, 0600, 1200, and 1800 UTC). Nevertheless, this finding suggests that the observed diurnal cycle of the cirrus category is not an instrumental effect (due to a decrease in the sensitivity of the lidar measurements). Liu and Zipser (2009) investigated the day versus night differences in water vapor and thin cloud observations near the tropical tropopause. They found that in the 16-km layer, clouds occur more frequently over Africa during night than during day; however, they did not separate the thin clouds observed in this layer as a function of their generation process. They found that the diurnal cycle of thin clouds, water vapor, deep convection, and the temperature are correlated in this layer. In our case we find a similar correlation, even if the thin anvil clouds directly detrained from convection are classified in the anvil category (in fact, Fig. 6 also shows the diurnal drought at the top of the anvil layer). Therefore, it may be argued that the observed diurnal cycle of cirrus clouds is more the result of the local diurnal variation of temperature in a saturated tropical tropopause layer. Inspection of the diurnal cycle of cirrus in the MSG classification also suggests such a diurnal cycle.

4. Radiative impact of cloud categories

Clouds strongly affect the radiation balance at the earth's surface by reducing the incident solar radiation, absorbing thermal infrared (IR) radiation emitted by the surface and the lower atmosphere, and emitting IR back to the surface. The net effect of clouds on the surface radiation balance depends significantly on cloud properties, surface properties, and solar elevation, as a function of latitude and season (Zhang et al. 1996). Over land, the incident solar radiation flux determines, in large part, the surface temperature and the rate of evapotranspiration, with important consequences on atmosphere–surface interactions and the global hydrological cycle. Cloud radiative forcing at the surface is defined as the difference between surface downward flux and clear-sky surface downward flux (Ramanathan et al. 1989). In this section the radiative forcing of the various cloud categories on shortwave and longwave fluxes at the surface is investigated.

a. Cloud radiative impact in the shortwave

The downwelling shortwave flux incoming at the surface depends on the first order of the sinus of the solar elevation angle and on scatter, absorption, and reflection (albedo effect) by clouds. In clear-sky conditions, the gaseous absorption (water vapor, ozone), Rayleigh scattering, absorption, and scattering by aerosols impact the atmosphere transmissivity. On the other hand, West Africa is notably subject to large smoke and mineral dust loads that can significantly modify the regional radiative budget (Li et al. 2004; Mallet et al. 2009). Indeed, the Sahara Desert acts as the strongest source of mineral dust aerosol in the world. Dust particles have a complex impact on the radiative transfer process

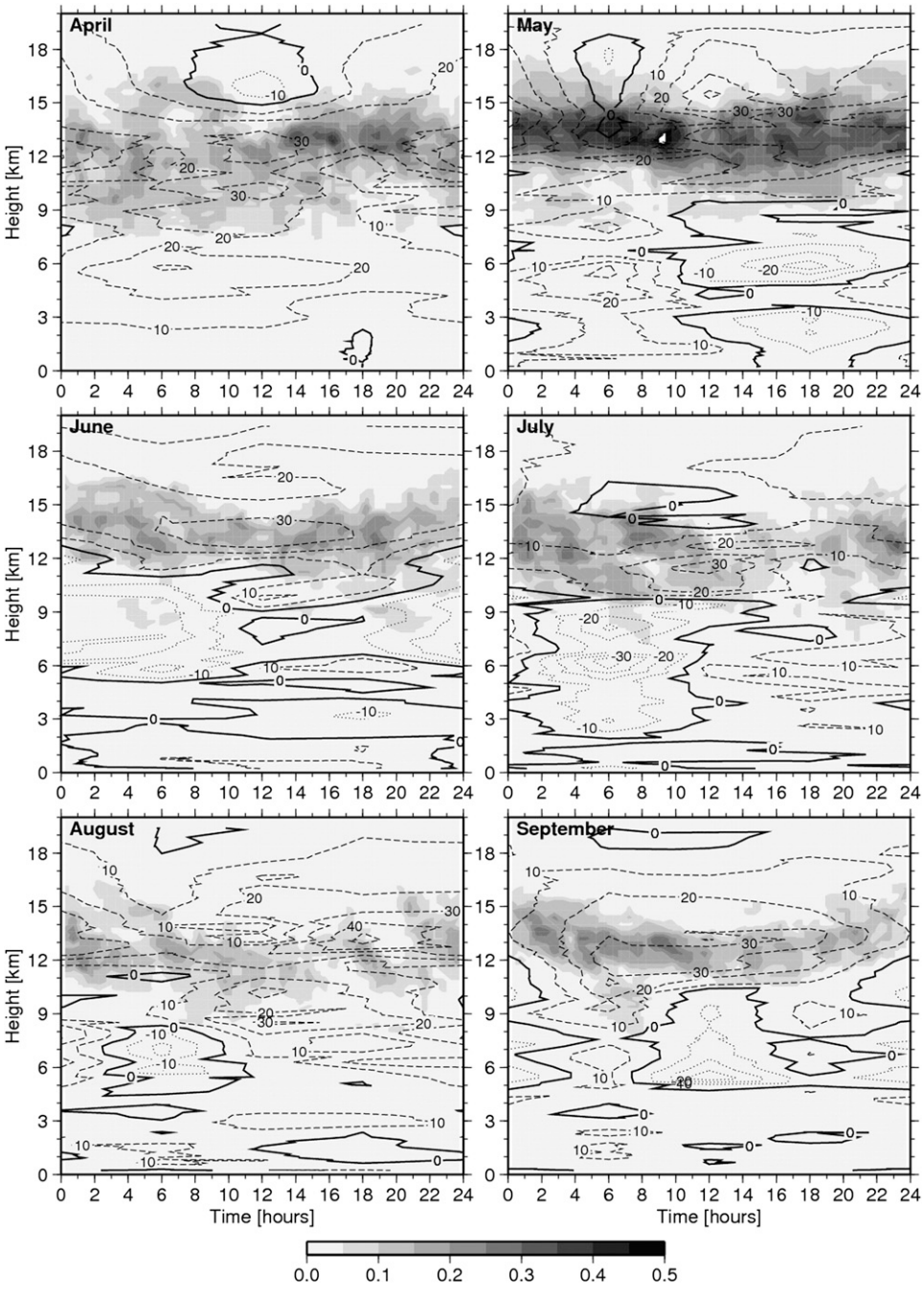

FIG. 8. Monthly diurnal cloud frequency of occurrence for the cirrus category from the AMF data (gray levels) with relative humidity anomaly superimposed (contour spacing 10%) interpolated from 6-hourly measurements, dashed for positive values and dotted for negative values, one panel per month. The zero contour is shown by the solid boldface line.

because of their ability to interact both in shortwave and longwave radiation.

To estimate the radiative forcing at the surface for each cloud category, it is first necessary to estimate the clear-sky shortwave downwelling flux. Two methods have been designed in order to quantify the clear-sky shortwave flux. Figure 9a illustrates both for a particular day (15 august 2006). As a first step, the measured shortwave flux is sorted according to the cloud (or clear sky) category previously defined (situations where several categories occur in the same column are not considered). This sorting is illustrated in Fig. 9a with for this

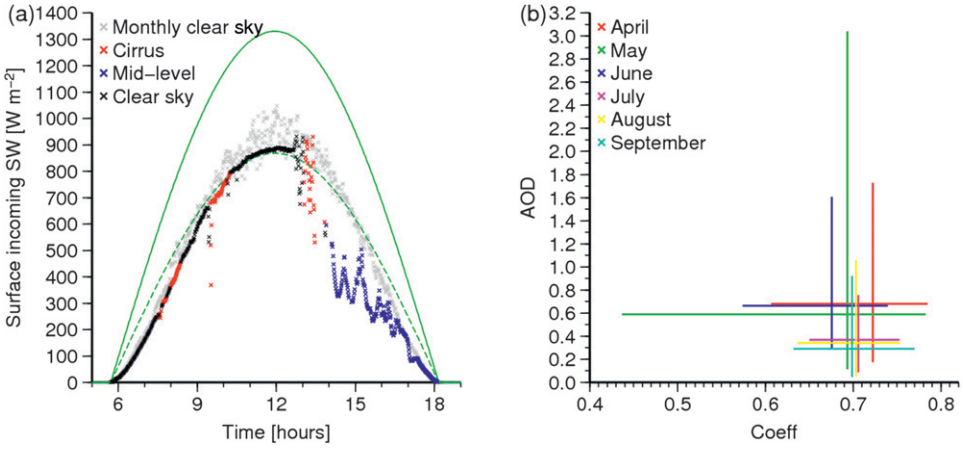

FIG. 9. Illustration of the retrieval of the shortwave cloud radiative forcing. (a) Downwelling shortwave flux at the surface on 15 Aug 2006, sorted according to the cloud category encountered in the atmospheric column: clear sky (black), cirrus (red), and midlevel clouds (blue). Gray crosses show the monthly composite of the clear-sky downwelling flux at the surface. The solid green line is the simulated incoming shortwave at the top of the atmosphere and the dashed green line is the same curve but fitted to the clear-sky measurements. (b) AOD as a function of the fitting coefficients (see text for explanation). For each month (one color per month), the vertical bars link the minimum and maximum values of AOD and the horizontal bars the minimum and maximum values of the fitting coefficient.

day two different cloud categories, cirrus and midlevel clouds; the remaining part of the day is characterized by clear sky. Around 1400 UTC midlevel clouds underlie the cirrus clouds. The corresponding profiles are not included in the analysis because the forcing of each cloud category would not be identifiable and no crosses appear in Fig. 9a at this time. The clear-sky points exhibit the expected sine shape with the solar elevation angle. However, the amplitude of this sine-shaped curve must be corrected for the clear-sky atmosphere transmissivity (including aerosol effects).

The first method for estimating clear-sky downwelling shortwave flux consists of simulating the shortwave flux at the top of the atmosphere (green curve in Fig. 9a) and then fitting it (dashed green curve) to the clear-sky measurements. The fitting coefficient value (corresponding to the transmissivity of the clear-sky atmosphere) is expected to depend strongly on the aerosol load of the particular day. As an example, the fitting coefficient is 0.6 for this day and an aerosol optical depth (AOD) of about 1 is measured by the Aerosol Robotic Network (AERONET) station located at Banizoumbou, Niger (about 50 km from Niamey), which is a rather large value for August. The main disadvantage of this method is that the fitting coefficient is considered constant for the entire day and that clear-sky measurements have to be present each day. The cloud radiative forcing is then computed only when the clear-sky flux has been determined. The second method consists of making the assumption that on a monthly scale one may build a composite of the clear-sky incoming shortwave radiation by averaging all the clear-sky measurements (at the time they were taken) obtained for the particular month. Figure 9a shows a composite for the month of August. It appears that the clear-sky measurements from 15 August 2006 (black crosses) contribute to a decrease in the incoming shortwave radiation for this month, likely because of a significant aerosol load for this day. By taking the difference with the same composites built for each cloud category, one assumes that the contributions of variations in the atmospheric state and aerosol load are minimized.

Figure 9b illustrates the seasonal evolution of the aerosol load in the Niamey area and the fitting coefficient's monthly variability. The mean values of the aerosol load and fitting coefficients may be separated into two families: April–June, which present large aerosol loads and a strong variability in the amount of aerosols present in the atmosphere, and July–September, with reduced load and variability. This reduced load may be explained by the occurrence during this period of precipitating events, which moisten the surface and scavenge the atmosphere, as well as the presence of vegetation at the ground, which prevents the emission of dust. In response to the larger variability during the premonsoon period, a larger variability is found for the fitting coefficients in comparison with the full monsoon season. A correlation coefficient can be computed between these two parameters leading to values from about −0.8 to −0.9 for the dry period that become from about −0.6 to −0.3

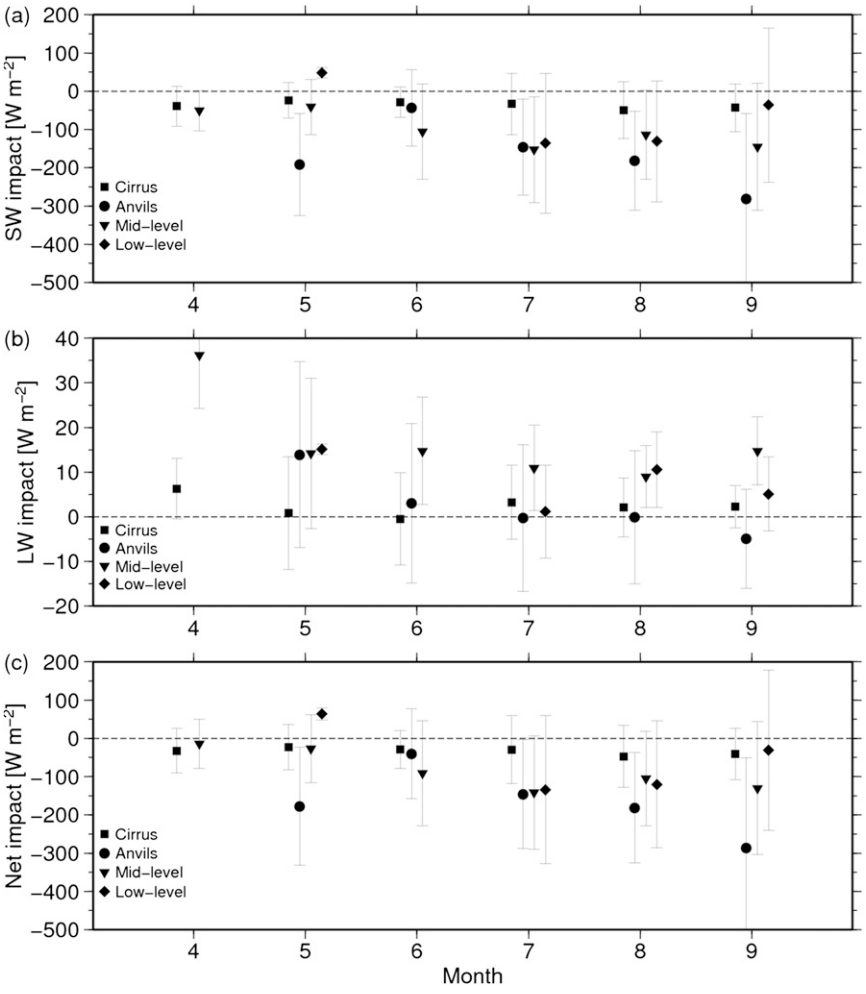

FIG. 10. Monthly mean (symbols) and standard deviation (vertical lines) of cloud radiative forcing at the surface deduced from AMF observations (a) in the shortwave, (b) in the longwave, and (c) for the net radiative impact (computed from diurnal composites).

for the wet season, showing that when strong aerosol events occur they are at the first order controlling the transmissivity of the clear-sky atmosphere.

Both methods have been applied to the present dataset. In the following, results from the second approach are mainly presented; however, the results from the first method lead to the same conclusions. Figure 10a shows the cloud radiative forcing in the shortwave radiation obtained by differencing the monthly composite of a given cloud category with the monthly composite in clear-sky situations. Each symbol represents a monthly mean value. It may be observed that all cloud categories have an impact on the shortwave results. For midlevel clouds a monthly decrease of incoming shortwave radiation between 50 and 150 W m^{-2} is found. The impact increases (in absolute value) as the monsoon migrates over the continent, suggesting a possible change in the cloud nature or a potential source of such clouds by deep convection, as suggested by Johnson et al. (1999). As expected, low-level clouds have a strong impact —a decrease of between 50 and 150 W m^{-2}. Note that we primarily consider here the wettest months (July–September), when a significant number of such clouds exists (see Fig. 4). This estimation is in good agreement with the cloud radiative forcing computed by Berg et al. (2011) for shallow cumuli sampled (-45.5 W m^{-2}) during summertime at the ARM's Southern Great Plains (SGP) site. Note that here and in the following, such comparisons are provided as a rough guide; the sun elevation angle, the atmospheric water vapor and temperature, and the amount and type of aerosols all differ among studies and these factors are also expected to modulate the impact of clouds on the surface incoming radiative fluxes.

Fairall et al. (2008) compute the cloud radiative forcing as the difference between measurements of all-sky flux in

the shortwave domain when shallow cumuli are present and the clear-sky radiative flux by using parameterizations tuned to accommodate regional and seasonal variability. Berg et al. (2011) also mention that at the same site Dong et al. (2006) estimated a forcing of -87.6 W m^{-2}, but they included all low-level cloud with a top lower than 3 km. The method used by Dong et al. (2006) to determine the clear-sky radiative flux is slightly different since they temporally interpolated the clear-sky measurements. The value found in this study (and its variability) is in the same range as in those former studies. Cirrus clouds (present ubiquitously all along the period) reduce the incoming shortwave of about 30–50 W m^{-2} (with a relative small month-to-month spread). Dupont and Haeffelin (2008) estimated the cloud radiative effect of various cirrus cloud types [using the same kind of methodology as Fairall et al. (2008)] and found an average reduction of 56 W m^{-2} at ground level for an observatory site located in western Europe. Using satellite data, Chen et al. (2000) found an average reduction of shortwave radiation of -22 W m^{-2}. Finally, anvil clouds present a strong impact, in particular for months of strong occurrence (July–September) where the decrease varies between 200 and up to 300 W m^{-2}. In radar–lidar observations, cirrus and nonprecipitating anvils may appear rather similar; however, when the cloud radiative forcing in the shortwave domain is considered, a radically different signal appears. The separation of the cirrus and anvil categories based on associated formation processes is therefore also justified for radiative purposes. Indeed, different microphysical properties are expected (large amount of small ice particles of about 15 μm for cirrus compared to larger ice particles in anvils) leading to differences in the radiative properties since a connection exists between cloud albedo, cloud emissivity, and ice water path (Stephens et al. 1990; Jensen et al. 1996).

The strong variability observed (even for a given cloud category) in the cloud radiative forcing is not a surprise since the present quantification does not take into account the detailed macrophysical properties of the cloud and in particular the cloud depth.

b. Cloud radiative impact in the longwave

In contrast to shortwave radiation, the longwave incoming flux at the surface does not vary much diurnally; however, the atmosphere transmissivity in the longwave domain is sensitive to the atmospheric gases, aerosols, and clouds. In particular, the abundance of moisture in the atmosphere makes the atmosphere strongly absorptive to the longwave radiation. Generally, clouds occur with saturation and therefore higher amounts of water vapor may be expected in the cloud vicinity. If one wants to properly estimate the cloud radiative forcing in the longwave domain, it would be necessary to estimate the incoming longwave flux in clear-sky situations on a day scale, which requires some knowledge of the temperature and water vapor fields. Within the framework of the AMMA project, this diurnal documentation is only poorly resolved with a maximum of four routine soundings per day (this number may reach eight for short particular periods). Another possibility is to compute the difference at the monthly scale between the incoming longwave radiation for each cloud category and the clear-sky composite as in the second method of the previous section. If we expect that this averaging would reduce the aerosol impact in the longwave domain, this may not be the case for atmospheric gases or for temperature. However, this method provides inferences on the cloud radiative forcing in the longwave domain (Fig. 10b). Note that for longwave radiation, it is only the monthly mean value (one symbol for each category) that is shown.

The vertical dashed line represents the standard deviation of the difference in the diurnal composite. Square symbols correspond to cirrus clouds, and, as may be expected from much earlier works (Manabe and Wetherald 1967; Cox 1971; Stephens and Webster 1981), they are generally associated with a small positive anomaly in the longwave domain that involves a heating of the troposphere owing to an increased emission to the surface by the cirrus layer (Stephens and Webster 1981). Dupont and Haeffelin (2008) estimated the cloud radiative effect of cirrus clouds at surface level for a midlatitude site (using a parameterization for the clear-sky fluxes and measurements for cloudy situations) and found values ranging from -6 up to 30 W m^{-2} with a mean impact near 5 W m^{-2}. The lower values (between 1 and 5 W m^{-2}) obtained here could be partly related to competing effects from aerosols and also the moister conditions encountered during the summer in the Sahel. The moisture effect may be more crucial to the radiative impact. Indeed, as the monsoon evolves to its mature stage, the integrated water path increases over the Sahel.

The enhancement of downwelling longwave flux induced by the clouds is reduced by enhanced absorption of the moister atmosphere below. This results in a downwelling longwave forcing at the surface that is only slightly larger than the clear-sky situation (e.g., Dong et al. 2006; Slingo et al. 2009). The slightly negative longwave cloud radiative forcing of anvils found in September may appear surprising though. Such a result cannot be interpreted solely in terms of cloud radiative forcing. Rather, it likely involves coupled fluctuations of temperature, water vapor, and clouds; in particular, the atmosphere associated with the large Sahelian anvils occurring at that time often displays strong cold anomalies. In addition, the longwave emission from the underlying wetted

surface is generally greatly reduced. Both factors contribute to a decrease in the surface incoming longwave flux. This finding clearly deserves further investigation.

Boundary layer clouds show a positive radiative forcing between 5 and 12 W m^{-2} in the moister part of the monsoon season. Such a positive cloud radiative forcing in the longwave domain was also diagnosed for shallow cumuli at the ARM SGP site with the same order of magnitude (15.9 W m^{-2}) by Berg et al. (2011). Chen et al. (2000) estimated the average impact (using satellite data and radiative transfer calculation) of cirrus clouds and low-level clouds and found larger values than in the present study (i.e., 8 and 39 W m^{-2}, respectively).

The midlevel clouds account for the largest positive impact (between 10 and 15 W m^{-2}). Since this category is rather ubiquitous, during the monsoon season a rather large impact may be expected on the energy balance and it would be interesting to determine if such clouds are well simulated by weather forecast and climate models and what their associated feedbacks are.

c. *Net cloud radiative impact*

The net cloud radiative impact is computed from the AMF data as the sum of the impacts in the short- and longwave domains. The results are shown in Fig. 10c. The main signal arising from this figure is the cooling effect of all cloud categories. This cooling remains modest up to the beginning of the migration of the ITCZ on the continent approximately in June, and then this cooling tends to be stronger. Since the cooling effect is mainly a result of the shortwave radiation, it dominates the net cloud radiative forcing during the monsoon season but not during the premonsoon period when the atmosphere is drier and less convective.

5. Conclusions

In this paper, ground-based and satellite observations during a monsoon season over West Africa have been used to characterize the cloud cover and radiative impact of clouds over this region. A particular use of the AMF radar–lidar ground-based measurements collected at the Niamey site has been to determine the different cloud categories occurring at this location, their diurnal cycle, and their seasonal evolution.

Four cloud categories are isolated from simple morphological considerations. As expected, convective clouds (generally leading to precipitations) and their related nonprecipitating anvils are found to be associated with the monsoon season. Low-level clouds occur during the wettest part of the monsoon. In contrast, two other cloud categories are found ubiquitously before and during the monsoon: midlevel and cirrus clouds (this cloud category frequency of occurrence is likely underestimated). Data from the A-Train *CloudSat–CALIPSO* satellites are used in order to highlight that these cloud categories are observable all over the West Africa region, along with stratocumulus clouds over the ocean.

The ground-based dataset is also used to document the diurnal cycle and its seasonal evolution for each cloud category. Each category presents a marked diurnal cycle that evolves all along the season. Although such a diurnal cycle were expected for low-level and convective clouds because their development is strongly related to surface processes (solar heating), it was rather unexpected for cirrus clouds.

Finally, the impact of each cloud categories on surface radiative fluxes has been investigated. Considerable attention has been paid in order to minimize the aerosol impact within the estimations. The largest reduction in incoming shortwave flux is found for the anvil category (between 200 and 300 W m^{-2}), low-level clouds and midlevel clouds both reduce the shortwave incoming flux by up to 150 W m^{-2}, and the impact of cirrus clouds may reach 50 W m^{-2}. These estimates should be taken and further combined with their frequency of occurrence since it has been shown for instance that cirrus clouds (even if they have the least impact) are ubiquitous throughout the season; this means that for all months the largest frequency of occurrence may well be underestimated (based on the satellite data examination).

In the longwave domain, the cloud radiative impact estimates remain qualitative since they are based on the available dataset and it is difficult to ensure that water vapor, temperature, and even aerosol contributions have been properly taken into account. The largest impact is found for midlevel and low-level clouds. More generally, the estimated values in shortwave and longwave domains are found to be in good agreement with the results from former studies available in the literature (Berg et al. 2011; Dupont and Haeffelin 2008; Dong et al. 2006; Chen et al. 2000) with a convergence of the orders of magnitude. However, little consideration has been paid to the macrophysical (e.g., cloud depth) and microphysical properties of the sampled clouds. As a next step, detailed calculations with a radiative transfer model should be performed in order to estimate more accurately the radiative forcing. The aim of the present paper was rather to show first that all the cloud categories present over this region have an impact on the surface radiative budget and that an accurate representation of cloudiness models is necessary in order to correctly simulate the energy budget. In particular, it seems that a proper representation of

midlevel clouds is critical because of their strong occurrence at regional scales, particularly over the Sahel and Sahara. From a physical-processes point of view or perspective, it would be particularly valuable to better understand and document the origins of these midlevel clouds. The ensemble of mechanisms behind their existence likely differs from those highlighted by Johnson et al. (1999) over the Pacific warm pool for congestus clouds. However, our study highlights the significance of this intermediate category of clouds across West Africa.

More generally, the present work contains an unprecedented documentation of cloud characteristics in a region where very little was known about clouds before 2006. Our research provides new diagnostics that can be further used to investigate whether numerical weather prediction and general circulation models are able to represent the observed characteristics, starting with their diurnal and seasonal patterns of evolution.

Finally, the present work, and in particular the spatial extension of the cloud radiative forcing quantification, are under investigation using the A-Train dataset and the present category sorting together with additional AMMA in situ datasets available along the meridional West African transect.

Acknowledgments. Based on a French initiative, AMMA was built by an international scientific group and is currently funded by a large number of agencies, especially from France, the United Kingdom, the United States, and Africa, and by an EU program. Detailed information on scientific coordination and funding is available on the AMMA International Internet site (http://www.amma-international.org). The Niamey AMF data were obtained from the Atmospheric Radiation Measurement (ARM) Program Archive of the Department of Energy. *CloudSat* data are obtained from CIRA of Colorado State University. ICARE and NASA gave access to the CALIOP data. This work was financially supported by CNES.

REFERENCES

Arnaud, Y., M. Desbois, and J. Maizi, 1992: Automatic tracking and characterization of African convective systems on Meteosat pictures. *J. Appl. Meteor.,* **31,** 443–453.

Berg, L. K., E. I. Kassianov, C. N. Long, and D. L. Mills Jr., 2011: Surface summertime radiative forcing by shallow cumuli at the Atmospheric Radiation Measurement Southern Great Plains site. *J. Geophys. Res.,* **116,** D01202, doi:10.1029/2010JD014593.

Betts, A. K., 2007: Coupling of water vapor convergence, clouds, precipitation, and land surface processes. *J. Geophys. Res.,* **112,** D10108, doi:10.1029/2006JD008191.

——, and P. Viterbo, 2005: Land-surface, boundary layer, and cloud-field coupling over the southwestern Amazon in ERA-40. *J. Geophys. Res.,* **110,** D14108, doi:10.1029/2004JD005702.

Boehm, M. T., and J. Verlinde, 2000: Stratospheric influence on upper tropospheric tropical cirrus. *Geophys. Res. Lett.,* **27,** 3209–3212.

Borovikov, A. M., and I. P. Mazin, and A. N. Nevzorov, 1978: Cloud structure peculiarities in the eastern zone of tropical Atlantic. *Proc. Int. Scientific Conf. on the Energetics of the Tropical Atmosphere,* Geneva, Switzerland, International Council of Scientific Unions/World Meteorological Society, 43–47.

Bouniol, D., and Coauthors, 2010: Using continuous ground-based radar and lidar measurements for evaluation of the representation of clouds in four operational models. *J. Appl. Meteor. Climatol.,* **49,** 1971–1991.

Cess, R. D., and Coauthors 1996: Cloud feedback in atmospheric general circulation models: An update. *J. Geophys. Res.,* **101** (D8), 12 791–12 794.

Chen, T., W. B. Rossow, and Y. Zhang, 2000: Radiative effects of cloud-type variations. *J. Climate,* **13,** 264–286.

Comstock, J. M., T. P. Ackerman, and G. G. Mace, 2002: Ground-based lidar and radar remote sensing of tropical cirrus clouds at Nauru Island: Cloud statistics and radiative impact. *J. Geophys. Res.,* **107,** 4714, doi:10.1029/2002JD002203.

Cox, S. K., 1971: Cirrus clouds and climate. *J. Atmos. Sci.,* **28,** 1513–1515.

Dessler, A. E., and P. Yang, 2003: The distribution of tropical thin cirrus clouds inferred from *Terra* MODIS data. *J. Climate,* **16,** 1241–1247.

Diongue, A., J.-P. Lafore, J.-L. Redelsperger, and R. Roca, 2002: Numerical study of Sahelian synoptic weather system: Initiation and mature stages of convection and its interactions with the large-scale dynamics. *Quart. J. Roy. Meteor. Soc.,* **128,** 1899–1927, doi:10.1256/003590002320603467.

Dong, X., B. Xi, and P. Minnis, 2006: A climatology of midlatitude continental clouds from the ARM SGP Central Facility. Part II: Cloud fraction and surface radiative forcing. *J. Climate,* **19,** 1765–1783.

Dufresne, J.-L., and S. Bony, 2008: An assessment of the primary sources of spread of global warming estimates from coupled atmosphere–ocean models. *J. Climate,* **21,** 5135–5144.

Dupont, J.-C., and M. Haeffelin, 2008: Observed instantaneous cirrus radiative effect on surface-level shortwave and longwave irradiances. *J. Geophys. Res.,* **113,** D21202, doi:10.1029/2008JD009838.

Duvel, J. P., 1989: Convection over tropical Africa and the Atlantic Ocean during northern summer. Part I: Interannual and diurnal variations. *Mon. Wea. Rev.,* **117,** 2782–2799.

Fairall, C. W., T. Utall, D. Hazen, J. Haire, M. F. Cronin, N. Bond, and D. E. Veron, 2008: Observations of cloud, radiation, and surface forcing in the equatorial eastern Pacific. *J. Climate,* **21,** 655–673.

Fiolleau, T., M. Tomasini, R. Roca, J.-P. Lafore, H. Laurent, T. Lebel, and K. Ramage, 2009: Summertime climatology of mesoscale convective systems over West Africa from 24-years of METEOSAT observations. *Geophysical Research Abstracts,* Vol. 11, Abstract ECU2009-9104.

Fueglistaler, S., A. E. Dessler, T. J. Dunkerton, I. Folkins, Q. Fu, P. W. Mote, 2009: Tropical tropopause layer. *Rev. Geophys.,* **47,** RG1004, doi:10.1029/2008RG000267.

Gamache, J. F., and R. A. Houze Jr., 1983: Water budget of a mesoscale convective system in the tropics. *J. Atmos. Sci.,* **40,** 1835–1850.

Garratt, J. R., 1993: Sensitivity of climate simulations to land-surface and atmospheric boundary-layer treatments—A review. *J. Climate,* **6,** 419–448.

Hartmann, D. L., J. R. Holton, and Q. Fu, 2002: The heat balance of the tropical tropopause, cirrus, and stratospheric dehydration. *Geophys. Res. Lett.,* **28,** 1969–1972.

Hayward, D., and J. Oguntoyinbo, 1987: *Climatology of West Africa.* Hutchinson Education, 271 pp.

Hogan, R. J., and E. J. O'Connor, cited 2010: Instrument synergy/target categorization. [Available online at http://www.cloud-net.org/data/products/categorize.html.]

——, C. Jakob, and A. J. I. Illingworth, 2001: Comparison of ECMWF winter-season cloud fraction with radar-derived values. *J. Appl. Meteor.,* **40,** 513–525.

Holle, R. L., J. Simpson, and S. W. Leavitt, 1979: GATE B-scale cloudiness from whole-sky cameras on four U.S. ships. *Mon. Wea. Rev.,* **107,** 874–895.

Hourdin, F., and Coauthors, 2009: AMMA-Model Intercomparison Project. *Bull. Amer. Meteor. Soc.,* **91,** 95–104.

Houze, R. A., Jr., 2004: Mesoscale convective systems. *Rev. Geophys.,* **42,** RG4003, doi:10.1029/2004RG000150.

——, and A. K. Betts, 1981: Convection in GATE. *Rev. Geophys.,* **19,** 541–576.

Illingworth, A. J., and Coauthors, 2007: Cloudnet: Continuous evaluation of cloud profiles in seven operational models using ground-based observations. *Bull. Amer. Meteor. Soc.,* **88,** 883–898.

Janicot, S., and Coauthors, 2008: Large-scale overview of the summer monsoon over West Africa during the AMMA field experiment in 2006. *Ann. Geophys.,* **26,** 2569–2595, doi:10.5194/angeo-26-2569-2008.

Jensen, E. J., O. B. Toon, H. B. Selkirk, J. D. Spinhirne, and M. R. Schoeberl, 1996: On the formation and persistence of subvisible cirrus clouds near the tropical tropopause. *J. Geophys. Res.,* **101,** 21 361–21 375.

Johnson, R. H., T. M. Rickenbach, S. A. Rutledge, P. E. Ciesielski, and W. H. Schubert, 1999: Trimodal characteristics of tropical convection. *J. Climate,* **12,** 2397–2418.

——, P. E. Ciesielski, T. S. L'Ecuyer, and A. Newman, 2010: Diurnal cycle of convection during the 2004 North American Monsoon Experiment. *J. Climate,* **23,** 1060–1078.

Kollias, P., M. A. Miller, K. L. Johnson, M. P. Jensen, and D. Troyan, 2009: Cloud thermodynamic, and precipitation observations in West Africa during 2006. *J. Geophys. Res.,* **114,** D00E08, doi:10.1029/2008JD010641.

Leary, C. A., and R. A. Houze Jr., 1979: Melting and evaporation of hydrometeors in precipitation from the anvil clouds of deep tropical convection. *J. Atmos. Sci.,* **36,** 669–679.

Le Barbé, L., T. Lebel, and D. Tapsoba, 2002: Rainfall variability in West Africa during the years 1950–90. *J. Climate,* **15,** 187–202.

Lebedeva, N. V., and N. A. Zavelskaya, 1980: Convection in the tropical ocean. *Conference on Scientific Results of GATE,* Kiev, USSR, Int. Council of Scientific Unions/World Meteorological Organization.

Lebel, T., and Coauthors, 2010: The AMMA field campaign: Multiscale and multidisciplinary observations in the West African region. *Quart. J. Roy. Meteor. Soc.,* **136** (S1), 8–33, doi:10.1002/qj.486.

Li, F., A. M. Vogelmann, and V. Ramanathan, 2004: Saharan dust aerosol radiative forcing measured from space. *J. Climate,* **17,** 2558–2571.

Liu, C., and E. Zipser, 2009: Implications of the day versus night differences of water vapor, carbon monoxide, and thin cloud observations near the tropical tropopause. *J. Geophys. Res.,* **114,** D09303, doi:10.1029/2008JD011524.

Mallet, M., P. Tulet, D. Serça, F. Solmon, G. Dubovik, J. Pelon, V. Pont, and O. Thouron, 2009: Impact of dust aerosols on the radiative budget, surface heat fluxes, heating rate profiles and convective activity over West Africa during March 2006. *Atmos. Chem. Phys.,* **9,** 7143–7160.

Manabe, S., and R. T. Wetherald, 1967: Thermal equilibrium of the atmosphere with a given distribution of relative humidity. *J. Atmos. Sci.,* **24,** 241–259.

Mather, J. H., and S. A. Mc Farlane, 2009: Cloud classes and radiative heating profiles at the Manus and Nauru Atmospheric Radiation Measurement (ARM) site. *J. Geophys. Res.,* **114,** D19204, doi:10.1029/2009JD011703.

Mathon, V., and H. Laurent, 2001: The life cycle of Sahelian mesoscale convective cloud systems. *Quart. J. Roy. Meteor. Soc.,* **127,** 377–406.

——, ——, and T. Lebel, 2002: Mesoscale convective system rainfall in the Sahel. *J. Appl. Meteor.,* **41,** 1081–1092.

Miller, M. A., A. Slingo, 2007: The ARM Mobile Facility and its first international deployment: Measuring flux divergence in West Africa. *Bull. Amer. Meteor., Soc.,* **88,** 1229–1244.

Peskow, B. E., 1980: Clouds and convection. *Conf. on Scientific Results of GATE,* Kiev, USSR, Int. Council of Scientific Unions/World Meteorological Organization.

Pfister, L., and Coauthors, 2001: Aircraft observations of thin cirrus clouds near the tropical tropopause. *J. Geophys. Res.,* **106** (D9), 9765–9786.

Protat, A., J. Delanoë, A. Plana-Fattori, P. May, and E. O'Connor, 2010: The statistical properties of tropical ice clouds generated by the West African and Australian monsoons from ground-based radar-lidar observations. *Quart. J. Roy. Meteor. Soc.,* **136,** 345–363, doi:10.1002/qj.490.

Ramanathan, V., R. Cess, E. Harisson, P. Minnis, B. Barkstrom, A. Ahmad, D. Hartmann, 1989: Cloud-radiative forcing and climate: Results from the Earth Radiation Budget Experiment. *Science,* **243,** 57–63.

Redelsperger, J.-L., A. Diongue, A. Diehdou, J.-P. Ceron, M. Diop, J.-F. Gueremy, and J.-P. Lafore, 2002: Multi-scale description of a Sahelian synoptic weather system representative of the West African monsoon. *Quart. J. Roy. Meteor. Soc.,* **128,** 1229–1257.

——, and Coauthors, 2006: AMMA, un projet international et multidisciplinaire de la mousson ouest-africaine. *La Météorologie,* **54,** 22–32.

Rickenbach, T., R. Nieto Ferreira, N. Guy, and E. Williams, 2009: Radar-observed squall line propagation and the diurnal cycle of convection in Niamey, Niger, during the 2006 African Monsoon and Multidisciplinary Analysis Intensive Observing Period. *J. Geophys. Res.,* **114,** D03107, doi:10.1029/2008JD010871.

Sassen, K., and B. S. Cho, 1992: Subvisual-thin cirrus clouds lidar data set for satellite verification and climatological research. *J. Appl. Meteor.,* **31,** 1275–1285.

Simpson, J., 1976: The GATE aircraft program: A personal view. *Bull. Amer. Meteor. Soc.,* **57,** 27–30.

Slingo, A., H. E. White, N. A. Bharmal, and G. J. Robinson, 2009: Overview of observations from the RADAGAST experiment in Niamey, Niger: 2. Radiative fluxes and divergences. *J. Geophys. Res.,* **114,** D00E04, doi:10.1029/2008JD010497.

Slingo, J., 1980: A cloud parameterization scheme derived from GATE data for use with a numerical model. *Quart. J. Roy. Meteor. Soc.,* **106,** 747–770.

Spinhirne, J. D., 1993: Micro pulse lidar. *IEEE Trans. Geosci. Remote Sens.,* **31,** 48–55.

Stephens, G. L., and P. J. Webster, 1981: Clouds and climate: Sensitivity of simple systems. *J. Atmos. Sci.,* **38,** 235–247.

——, S.-C. Tsay, P. W. Stackhouse Jr., and P. J. Flatau, 1990: The relevance of the microphysical and radiative properties of cirrus clouds to climate and climatic feedback. *J. Atmos. Sci.,* **47,** 1742–1753.

——, and Coauthors, 2002: The CloudSat mission and the A-Train: A new dimension of space-based observations of clouds and precipitation. *Bull. Amer. Meteor. Soc.,* **83,** 1771–1790.

Stokes, G. M., and S. E. Schwartz, 1994: The Atmospheric Radiation Measurement (ARM) Program: Programmatic background and design of the cloud and radiation test bed. *Bull. Amer. Meteor. Soc.,* **75,** 1201–1221.

Sultan, B., and S. Janicot, 2003: The West African monsoon dynamics. Part II: The ''preonset'' and the ''onset'' of the summer monsoon. *J. Climate,* **16,** 3407–3427.

——, and ——, 2000: Abrupt shift of the ITCZ over West Africa and intra-seasonal variability. *Geophys. Res. Lett.,* **27,** 3353–3356.

Winker, D., W. Hunt, M. McGill, 2007: Initial performance assessment of CALIOP. *Geophys. Res. Lett.,* **34,** L19803, doi:10.1029/2007GL030135.

Xi, B., X. Dong, P. Minnis, and M. M. Khaiyer, 2010: A 10-year climatology of cloud cover and vertical distribution derived from both surface and GOES observations over the DOE ARM SGP site. *J. Geophys. Res.,* **115,** D12124, doi:10.1029/2009JD012800.

Zhang, T., K. Stammes, and S. A. Bowling, 1996: Impact of clouds on surface radiative fluxes and snowmelt in the Arctic and subarctic. *J. Climate,* **9,** 2110–2123.

Zheng, X., and E. A. B. Eltahir, 1998: The role of vegetation in the dynamics of West African monsoons. *J. Climate,* **11,** 2078–2096.